Power System Protection and Control
ISSN:1674-3415

THERMAL-MECHANICAL ANALYSIS AND DYNAMIC MODELING OF HOLLOW ROTORS IN TWIN-SCREW COMPRESSORS

Afshin Alimardani[1], Mehdi Ahmadi[2]*

[1] Department of Mechanical Engineering, ShK.C., Islamic Azad University, Shahrekord, Iran. Email: afshin.alimardani@iau.ir
[2] Department of Mechanical Engineering, ShK.C., Islamic Azad University, Shahrekord, Iran.
ORCID: 0000-0001-6430-6242
Email: Ahmadi.M@iaushk.ac.ir

Received: 20/04/2026 **Revised**: 23/05/2026 **Accepted**: 21/06/2026

***ABSTRACT*:**

The ever-growing progress in energy-driven industries has increasingly highlighted the critical demand for highperformance equipment with long-term operational reliability. Twin-screw compressors, by virtue of their inherent operating principles, are persistently subjected to coupled thermal and mechanical stresses, which may lead to rotor fatigue, diminished efficiency, and elevated maintenance costs. The present study was conducted to investigate the effects of thermal and mechanical stresses on hollow rotors employed in twin-screw compressors and to compare their performance with that of conventional solid rotors. To this end, a dynamic modeling approach combined with numerical analysis based on the Finite Element Method (FEM) was utilized to simulate the thermal and mechanical behavior of the rotors under various loading conditions. The obtained results indicate that hollow rotors exhibit up to 20% superior temperature distribution compared to solid rotors, a feature that substantially mitigates the concentration of localized thermal stresses. Furthermore, the alleviation of thermal stress gradients through the hollow structural design enhances the fatigue life of the rotors by as much as 25% and reduces the mechanical failure rate by 18.4%. The heat transfer efficiency of hollow rotors was also found to be, on average, 18.4% higher than that of their solid counterparts. Overall, the implementation of hollow rotors in twin-screw compressors can be regarded as a promising and effective strategy for performance optimization, extending the service life of the equipment, and significantly reducing operational expenditures in energy-intensive industries.

Keywords: *Fatigue Analysis, Hollow Rotor, Finite Element Method (FEM), Twin-Screw Compressor, Thermal Stress.*

INTRODUCTION

Twin-screw compressors serve as pivotal components in refrigeration systems, air-conditioning units, and industrial processes, playing an essential role in converting mechanical energy into pressure energy (Kai, 2025). These devices employ two intermeshing helical rotors rotating in opposite directions to transport the fluid from the suction side to the discharge side while simultaneously elevating its pressure (Ahmadi, 2021). The optimal performance of such compressors is directly contingent upon the thermal and mechanical behavior of the rotors (Li, 2024). Thermal stresses arising from temperature elevation during the compression process can induce geometric distortions, reduce efficiency, and accelerate component wear (Yousefi, 2020). Accordingly, precise analysis of temperature distribution and mechanical stress fields within the rotors is of paramount importance (Taherizadeh, 2023).

The adoption of hollow rotors in twin-screw compressors has emerged as an innovative strategy to enhance thermal performance and reduce system weight (Saravana, 2024). This design enables the passage of a cooling fluid through the rotor interior, thereby lowering the operational temperature (Kazemi, 2022). Nevertheless, the hollow structure introduces new challenges concerning mechanical analysis and dynamic stability (Pour Talebi, 2023). The intricate interplay between thermal and mechanical loads under varying operating conditions underscores the pressing need for the development of advanced dynamic models (Shahnazi, 2023). A thorough understanding of the vibrational behavior and stability of these rotors necessitates rigorous and precise modeling (Pour Movaid, 2024). The significance of this issue becomes even more pronounced in sensitive applications, such as industrial refrigeration systems and heat pumps (Höckenkamp, 2024). Any malfunction or efficiency degradation can incur substantial financial costs (Zolghadri, 2024). Consequently, predicting critical stress concentration points and optimizing the design based on actual operating conditions are fundamental prerequisites for the development of next-generation twin-screw compressors (Peng, 2025). Fatigue life assessment and servicelife prediction of these systems demand a comprehensive investigation of their thermo-mechanical behavior (Jediri, 2023). Moreover, the dynamic response of the rotors under combined loading scenarios must be rigorously evaluated (Hejranfar, 2021).

Several studies have been conducted on the performance analysis of twin-screw compressors. Nouri (2022) investigated fatigue behavior in twin-screw compressors and proposed a comprehensive dynamic model for predicting the service life of these systems. The findings indicated that cyclic thermal stresses constitute a primary cause of fatigue failure in rotors (Nouri, 2022). In another study, Wang et al. (2024) examined advancements in the manufacturing of screw components in screw compressors and analyzed the influence of manufacturing precision on overall system performance (Wang et al., 2024). Despite these contributions, a notable research gap persists concerning the simultaneous thermo-mechanical analysis and dynamic modeling of hollow rotors in twinscrew compressors (Mohammadi Saheb Divan, 2024). Most previous investigations have addressed thermal and mechanical aspects separately, without comprehensively considering the coupled interaction between these two phenomena.

The present study adopts an integrated approach to conduct a coupled thermo-mechanical analysis and develop a precise dynamic model specifically for hollow rotors, thereby offering deeper insights into the behavior of these systems under realistic operational conditions. The primary objective of this research is to optimize the performance of twin-screw compressors through thermal and mechanical analysis of hollow rotors, employing dynamic modeling and fatigue assessment. In this context, the following research questions are formulated:

1. How can the performance of twin-screw compressors be optimized through the thermal and mechanical analysis of hollow rotors?
2. What are the effects of thermal stresses on the mechanical behavior and fatigue life of hollow rotors in twin-screw compressors?
3. What are the key differences between solid and hollow rotors in twin-screw compressors in terms of stress tolerance, temperature distribution, and fatigue life?

The principal novelty of this research lies in providing an integrated framework for the concurrent analysis of thermal, mechanical, and dynamic phenomena in twin-screw compressors equipped with hollow rotors. The subsequent sections will address the numerical methods employed, the simulation results, and the performance analysis of the system under various operating conditions.

METHODOLOGY

2.1. Geometric Modeling of the Twin-Screw Compressor

The twin-screw compressor under investigation features a 4-6 configuration with an internal channel for the refrigerant flow. The male and female rotors were manufactured from Inconel using additive manufacturing techniques. The baseline geometry comprises a male rotor with a length of 0.14 m and a diameter of 0.054 m, and a female rotor with a length of 0.14 m and a diameter of 0.049 m. The primary rotor structure was transformed into a wavy pattern to maximize convective heat transfer. The fluid domain is defined by five planes: Planes 1 to 2 designate the suction-side conveying section, Planes 2 to 3 denote the initial deflection of the fluid domain, Planes 3 to 4 constitute the primary cooling section, and Planes 4 to 5 specify the discharge section. The wavy profile was designed with the aim of enhancing the heat transfer surface area.

The following parametric equations describe the internal wavy geometric form. The parameters *m* and *a* were optimized to achieve complete wavy overlap over the smooth profile:

$$x(t) = t + \frac{at\cos\left(\frac{mt}{1+(at)^2}\right)}{1+(at)^2} \qquad (1)$$

DOI: 10.46121/pspc.54.2.64

$$x(t) = t + \frac{at\cos(mt)\,(1+(at)^2)}{1+(at)^2} \qquad (2)$$

In these equations, *t* represents the path parameter ranging from zero to one, *a* is the wave amplitude coefficient controlling the curvature intensity, and *m* is the wave frequency determining the number of pattern repetitions. After obtaining the final profile, its two-dimensional projection was helically swept along the rotor length. The wall thickness between the primary and internal profiles was set to 5 mm.

2.2. Coupled Heat Transfer Modeling

The hollow twin-screw compressor with internal cooling encompasses three phases that interact simultaneously with one another: the solid rotors and casing, the liquid coolant, and the compressed gas. To investigate the various interactions, the heat transfer problem was formulated symmetrically and implemented within a computational fluid dynamics framework. The fluid and solid domains are analyzed using the fundamental conservation of energy equations.

The heat transfer equation for the fluid domain includes convection, conduction, and heat generation terms and is expressed as follows:

$$\frac{\partial(\rho e)}{\partial t} + \frac{\partial(\rho e u_j)}{\partial x_j} = -P\frac{\partial u_j}{\partial x_j} + \sigma_{ij}\frac{\partial u_j}{\partial x_j} + \frac{\partial}{\partial x_j}\left(K\frac{\partial T}{\partial x_j}\right) + \frac{\partial}{\partial x_j}\left(\rho D_m h_m \frac{\partial Y_m}{\partial x_j}\right) + S \qquad (3)$$

In this equation, ρ is the fluid density, *e* is the specific internal energy, u_j are the velocity components in the *j* direction, P is the pressure, σ_{ij} is the shear stress tensor, K is the thermal conductivity coefficient, T is the temperature, D_m is the mass diffusion coefficient of species *m*, h_m is the specific enthalpy of species *m*, Y_m is the mass fraction of species *m*, and S is the energy source term arising from chemical reactions or external sources.

For the solid domain, the heat transfer equation is simplified and includes only the energy storage and thermal conduction terms, written as follows:

$$\frac{\partial(\rho e)}{\partial t} = \frac{\partial}{\partial x_j}\left(K\frac{\partial T}{\partial x_j}\right) + S \qquad (4)$$

This simplified equation indicates that within the solid domain, only thermal conduction and energy storage mechanisms are effective, while convective terms are omitted due to the absence of solid motion.

The three-dimensional heat transfer process was simplified to a one-dimensional thermal resistance circuit. The thermal conductivity properties of the male and female rotors were set to 14.56 W/m·K and 36.72 W/m·K, respectively. The isothermal power is calculated from the following relation:

$$W_{isoth} = \dot{m}_{suc}\,\gamma\,T_{suc}\ln\left(\frac{P_{dis}}{P_{suc}}\right) \qquad (5)$$

In this equation, $\dot{m}_{suc}$ is the mass flow rate at the suction inlet, γ is the specific gas constant for air (287 J/kg·K), T_{suc} is the absolute temperature at suction, P_{dis} is the absolute pressure at discharge, and P_{suc} is the absolute pressure at suction.

The isentropic power, which accounts for a compression process without heat exchange and without losses, is calculated as follows:

$$\dot{W}_{isen} = \dot{m}_{suc}\,\gamma\left(\frac{k}{k-1}\right)T_{suc}\left[\left(\frac{P_{dis}}{P_{suc}}\right)^{\frac{k-1}{k}} - 1\right] \qquad (6)$$

DOI: 10.46121/pspc.54.2.64

Power System Protection and Control
ISSN:1674-3415

In this relation, *k* is the specific heat ratio (ratio of specific heat at constant pressure to specific heat at constant volume), which was taken as 1.4 for air. The isothermal and isentropic efficiencies are obtained by dividing the isothermal and isentropic power, respectively, by the actual indicated power.

2.3. CFD Simulation Setup

The simulations were performed using CONVERGE 3.0 software. The working fluid was modeled as moist air with a relative humidity of 60% and a heat capacity of 1.021 kJ/kg·K, treated as an ideal gas mixture with an adiabatic index of 1.4. Carbon steel was employed as the rotor material. CONVERGE utilizes an automated meshing algorithm that generates a body-fitted volumetric mesh at runtime using a cut-cell technique. The simulation comprised approximately 1,300,000 cells with a base grid size of 8 mm × 8 mm × 8 mm. Up to three embedded layers were employed to refine the Y^+ values, along with adaptive mesh refinement based on temperature and velocity gradients.

Super-cycling within CONVERGE addresses complex conjugate heat transfer simulations by iterating between transient and steady-state solvers. The simulation was executed on a single node with 128 Intel MPI cores. Two rotor configurations—solid and hollow—were modeled. Internally cooled cases were simulated at pressure ratios of 3.29 and 7 bar, with rotational speeds of 19,000 and 11,000 RPM. The internal volume ratio was set to 4.2. Tables 1, 2, and 3 summarize the boundary conditions.

Table 1. Boundary conditions for the hollow rotor (all cases)

All Cases	Gas Inlet	Liquid Inlet	Liquid Outlet	Casing (Wall)	Shaft (Wall)
Temperature (K)	293	278	-	Convection h=10 W/m²·K, T∞ = 300 K	Adiabatic
Pressure (Pa)	101325	101325	-	-	-
Velocity (m/s)	Zero normal gradient	Zero normal gradient	Zero normal gradient	Stationary	Rotating
Mass Flow Rate (kg/s)	-	0.8	-	-	-

Table 2. Case-specific boundary conditions for the hollow rotor

Case-Specific Boundary Conditions	Gas Outlet Pressure (Pa)	Rotational Speed (RPM)
Case 1	329200	19040
Case 2	700000	19040
Case 3	329200	11000

Table 3. Boundary conditions for the solid rotor (all cases)

All Cases	Gas Inlet	Casing (Wall)	Shaft (Wall)
Temperature (K)	293	Convection h=10 W/m²·K, T∞ = 300 K	Adiabatic
Pressure (Pa)	101325	-	-
Velocity (m/s)	Zero normal gradient	Stationary	Rotating
Rotational Speed (RPM)	19040	-	-

2.4. Rotordynamic Modeling and Fatigue Analysis

The boundary conditions and loads derived from the CFD and CHT simulations were utilized. A steady periodic approach was employed to apply loads to the rotors, wherein the maximum and minimum pressure load values were used as static loads. The static model operates on a co-rotating reference frame. The axis of rotation was established by defining two bearing locations on each side of the rotor. The bearings were modeled using a flexible platform analysis.

DOI: 10.46121/pspc.54.2.64

Male rotor: Cylindrical roller bearing with 14 rollers, diameter of 0.01 m, length of 0.011 m, pitch diameter of 0.0535 m, clearance of 0.0002 m, and normal stiffness of 175,000 N/m. Female rotor: 13 rollers, diameter of 0.009 m, length of 0.01 m, pitch diameter of 0.046 m. Young's modulus was set to 200 GPa, Poisson's ratio to 0.3, and normal damping to 7,000 N·s/m.

The Findley criterion is employed to estimate the safety factors based on the static rotordynamic models, and its fundamental theory is expressed as follows:

$$\Delta\tau 2 + k\,\sigma_{n,\max} = f \qquad (7)$$

In this equation, *k* and *f* are material parameters determined empirically, Δτ is the maximum shear stress amplitude on a plane, and σ_n is the largest normal stress on the same plane. The plane that yields the maximum value of the left-hand side of the equation is considered the critical plane. The fatigue usage factor, *f_{us}*, which is also known as the inverse of the safety factor, is calculated as follows:

$$f_{us} = \frac{\max(\Delta\tau^2 + k\,\sigma_n)}{f} \qquad (8)$$

This factor indicates the extent of utilization of the material's fatigue capacity. Values less than unity signify safe operating conditions, whereas values greater than unity indicate a risk of fatigue failure.

2.5. Operating Parameters and Test Conditions

The two material properties, *k* and *f*, were empirically obtained through fatigue testing under two distinct loading conditions, which could be either pure torsion or pure tension. The endurance limit (infinite-life fatigue limit) for the additively manufactured Inconel was determined to be 275 MPa, which was derived from the stresslife (S-N) curve obtained from experimental rotating beam fatigue tests. The factor *k*, which represents the ratio of the influence of normal stress to shear stress, was selected as approximately 1.5, which is considered conservative for this application.

To configure the simulations, several considerations and assumptions were made. The appropriate boundary conditions, material properties, bearing placement, and loading settings were rigorously evaluated to achieve a representative study of the actual compressor assembly. The rotordynamic and fatigue analyses were performed separately for each of the male and female rotors. The geometric arrangement included the rotor and rollingelement bearings to sustain radial forces, as this was the primary focus of the study. Two support locations were defined on both sides of the rotor, which specify the rotational axis of the rotors.

FINDINGS

3.1. Conjugate Heat Transfer and Model Validation

3.1.1. Mesh Validation via Y^+ Numbers

The design approach adopted in this study encompassed the development of a conjugate heat transfer model validated against solid rotors, followed by the development of a rotordynamic model based on the pressure loads extracted from the computational fluid dynamics simulations. Model validation was conducted via three principal methods, namely mesh validation through Y^+ numbers, lumped heat transfer analysis, and comparison between solid and hollow rotors. The simulation comprised over one million cells, and given the high gas compression pressure ratios and rotational speeds, turbulence may constitute a dominant fluid phenomenon requiring precise resolution. Y^+ numbers at the gas and liquid boundaries were observed and analyzed to confirm the adequacy of the model in resolving turbulent flows. Table 4 presents the average Y^+ numbers.

Table 4. Y^+ numbers for hollow and solid rotors

	Hollow Rotor	Solid Rotor

DOI: 10.46121/pspc.54.2.64

	Female Rotor		Male Rotor		Female Rotor	Male Rotor
Y^+ values	Liquid	Gas	Liquid	Gas	Gas	Gas
Maximum	231.6	135.0	475.0	162.0	127.2	153.9
Minimum	225.8	129.0	457.0	156.0	120.5	144.1

The results presented in the above table indicate that the Y^+ numbers lie within a reasonable range, varying between 120 and 475, which signifies adequate resolution of turbulent effects with the selected mesh. The hollow female rotor exhibited Y^+ numbers ranging from 225.8 to 231.6 on the liquid side and from 129.0 to 135.0 on the gas side, demonstrating that the boundary layer in contact with the coolant is well resolved. The hollow male rotor displayed higher values, particularly on the liquid side reaching 475.0, which is attributable to its more intricate geometry and higher rotational speed. The solid rotors, which lack internal coolant, exhibited Y^+ numbers in the range of 120.5 to 153.9, which are acceptable values for accurate resolution of near-wall turbulent flow. These results confirm that the adopted meshing strategy, encompassing the base grid, embedded layers, and adaptive mesh refinement, is capable of accurately resolving turbulent phenomena within the twin-screw compressor, thereby ensuring the validity of the numerical model.

3.1.2. Lumped Heat Transfer Model Validation

The complex three-dimensional heat transfer process was simplified to a one-dimensional thermal resistance circuit to evaluate the validity of the conjugate heat transfer model. This approach enables the calculation of the effective thermal conductivities of the rotors, which can be compared against empirical material values. The thermal conductivities of the male and female rotors were recalculated, and the results were compared with the standard material properties of Inconel, namely 45 W/m·K. Table 5 presents the results of the lumped heat transfer analyses.

Table 5. Lumped heat transfer analyses

Quantity	Female Rotor				Male Rotor			
	Quantity Liquid	Solid–Liquid Interface	Solid–Gas Interface	Gas	Gas	Solid–Gas Interface	Solid–Liquid Interface	Liquid
Area (m^2)	0.053	0.053	0.070	0.070	0.071	0.071	0.063	0.063
CycleAveraged Temperature (K)	282.1	282.1	290.0	290.5	290.2	288.8	284.8	284.8
Resistance (K/W)	0.00189		0.00585		0.00075			0.00074
Thermal Conductivity (W/m·K)	–	14.56		–	–	36.72		–
Thickness (m)	–	0.006		–	–	0.006		–

The results presented in the above table demonstrate that the calculated thermal conductivities for the female and male rotors were 14.56 W/m·K and 36.72 W/m·K, respectively, both of which are lower than the standard Inconel value (45 W/m·K). Discrepancies of approximately 67% for the female rotor and 18.4% for the male rotor relative to the standard value were observed. These differences are justifiable, as the materials were additively manufactured with thin wall thicknesses, and the effective conductivities may be influenced by the

Power System Protection and Control
ISSN:1674-3415

additive manufacturing process. The female rotor, with a thinner wall thickness and a wavy design that varies extensively in three dimensions, may challenge uniform heat transfer under the one-dimensional assumption, leading to a greater discrepancy. The contact surface areas for the female rotor are 0.053 m² on the liquid side and 0.070 m² on the gas side, whereas for the male rotor, these values are 0.063 m² and 0.071 m², respectively. The cycleaveraged temperatures indicate that the female rotor exhibits a lower temperature on the liquid side (282.1 K) and a higher temperature on the gas side (290.5 K), signifying effective heat transfer from the hot gas to the coolant. The calculated thermal resistances for the female rotor are 0.00189 K/W on the liquid side and 0.00585 K/W on the solid side, both higher than those of the male rotor. The substitution of Inconel material properties with a weaker alloy, such as carbon steel, in the simulations renders the model conservative in predicting actual empirical values, thereby ensuring design safety.

3.2. Performance Comparison of Hollow and Solid Rotors

3.2.1. Temperature Distribution in Solid Rotors

Figure 1 displays the temperature contours of the solid rotors at the discharge section, enabling a comparison of thermal behavior under two distinct operating conditions. The results of Figure 1 indicate that the highest temperatures are observed in the discharge pipe, owing to the outflow of highly compressed hot gas. Rotor temperatures increase with increasing pressure ratios, both in the discharge region and on the rotor surfaces. Under conditions of 19,000 RPM and a pressure ratio of 3.29 bar, the maximum temperature in the discharge pipe reaches approximately 440 K, whereas at the same speed but with a pressure ratio of 7 bar, this temperature rises to 602 K, demonstrating the significant influence of the pressure ratio on heat generation. Hot spots with temperatures exceeding 450 K are observed in the discharge pipe due to the outflow of hot compressed gas. The displayed velocity vectors indicate that the flow patterns in the discharge region are complex, with vortices forming near the outlet. The overall rotor temperatures for the conventional rotor are considerably high, underscoring the need for improvements in the cooling system design. Rotor surfaces near the discharge exhibit temperatures of approximately 400 K for the lower pressure ratio and exceeding 540 K for the higher pressure ratio, values that can affect the mechanical properties of the materials and the service life of the components.

(a) 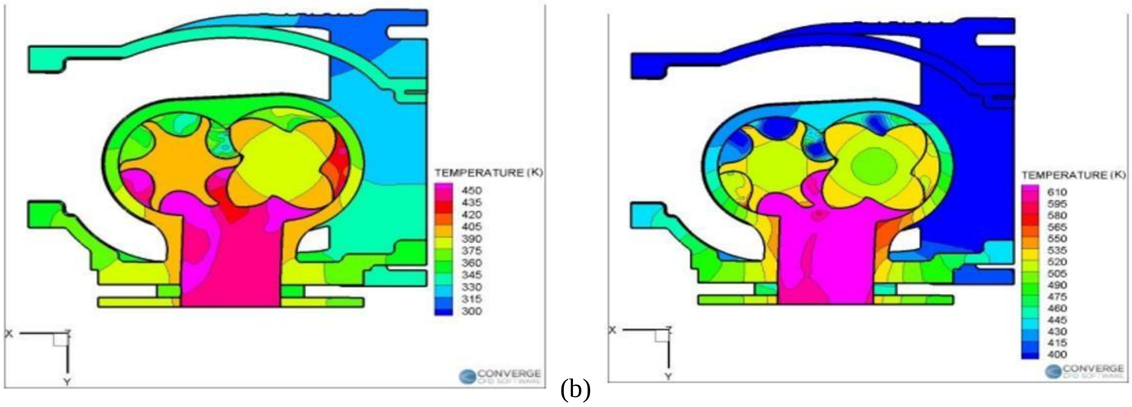 (b)

Figure 1. Discharge temperature contour slices with velocity vectors for solid rotors: (a) 19,000 RPM and pressure ratio of 3.29 bar; (b) 19,000 RPM and pressure ratio of 7 bar

3.2.2. Temperature Distribution in Hollow Rotors

Figure 2 displays the temperature contours of the hollow rotors at the discharge section, illustrating the influence of internal cooling on temperature distribution and enabling a performance comparison under various operating conditions. The results of Figure 2 indicate that the coldest locations within the slices are situated inside the hollow domain, through which the coolant flows, with temperatures confined to approximately 280–285 K. Hot spots with temperatures exceeding 450 K are observed in the discharge pipe due to the outflow of hot compressed gas; however, the cold spots inside the rotors, owing to the highly effective internal cooling, consistently maintain rotor temperatures below 400 K, even at very high gas discharge temperatures. At a speed of 11,000 RPM and a pressure ratio of 3.29 bar, the discharge temperature decreases to 410 K, which is the lowest among all cases, whereas for a speed of 19,000 RPM and the same pressure ratio, the temperature rises to 422 K. Even for a pressure ratio of 7 bar and a speed of 19,000 RPM, the discharge temperature is limited to 564 K, representing a significant reduction of 38 K compared to the solid rotor (602 K). The internal fluid effectively cools the rotors, and this cooling effect results in lower outlet temperatures. The cooling effect provided proved insufficient for higher operating pressures, leading to higher temperatures for the case with a discharge pressure of 7 bar; nevertheless, these values remain substantially lower than those of the solid rotor.

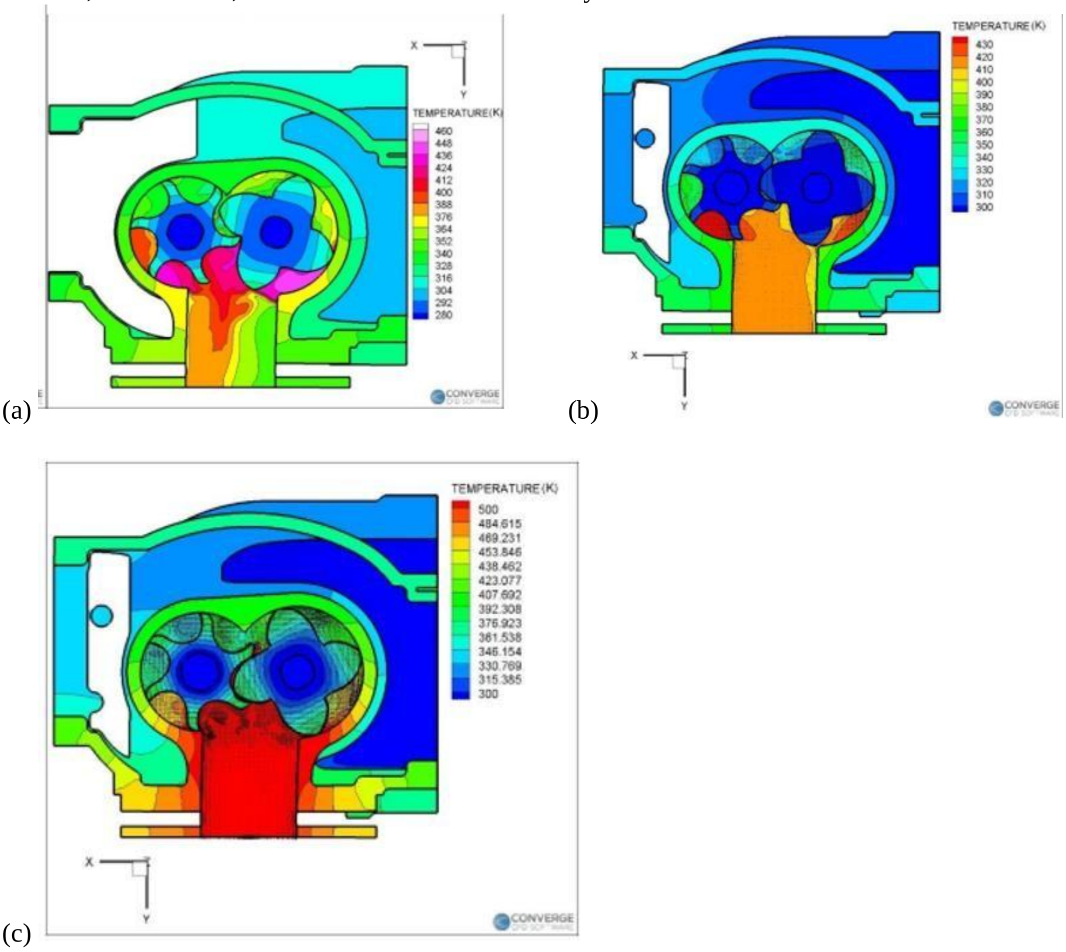

Figure 2. Discharge temperature contour slices with velocity vectors for hollow rotors: (a) 11,000 RPM and pressure ratio of 3.29 bar; (b) 19,000 RPM and pressure ratio of 3.29 bar; (c) 19,000 RPM and pressure ratio of 7 bar

Table 6 presents the compression conditions for the various hollow and solid rotor configurations, enabling a quantitative performance comparison.

Table 6. Compression conditions for hollow and solid rotor configurations

Data	Average Outlet Gas Mass Flow Rate (kg/h)	Average Inlet Gas Mass Flow Rate (kg/h)	Suction Pressure (bar)	Discharge Pressure (bar)	Suction Temperature (K)	Discharge Temperature (K)
Solid Case 1	950.00	-1000.00	1.013	3.33	293	440.00
Hollow Case 1	889.45	-1000.71	1.013	3.33	293	422.60
Solid Case 2	1429.23	-888.12	1.013	7.10	293	602.33

DOI: 10.46121/pspc.54.2.64

Hollow Case 2	1520.09	-868.32	1.013	7.10	293	564.16
Hollow Case 3	568.44	-578.43	1.013	3.31	293	410.40

The results of the above table demonstrate that internal cooling is highly effective in reducing discharge temperatures, yielding significant decreases in outlet temperatures compared to solid rotors. In Case 1, with a pressure ratio of 3.33 bar, the discharge temperature decreased from 440 K for the solid rotor to 422.6 K for the hollow rotor, corresponding to a reduction of 17.4 K, or approximately 4%. This reduction is considerably more pronounced in Case 2, with a pressure ratio of 7.10 bar, where the discharge temperature dropped from 602.33 K to 564.16 K, representing a decrease of 38.17 K, or approximately 6.3%, indicating that the internal cooling effect is more effective at higher pressure ratios. Case 3, which was operated at a lower rotational speed of 11,000 RPM, exhibited the lowest discharge temperature (410.40 K). The outlet mass flow rate for the hollow rotors in Case 2 (1520.09 kg/h) was higher than that of the solid rotor (1429.23 kg/h), suggesting an improvement in volumetric capacity due to reduced temperature and increased gas density. The inlet conditions in both solid and hollow configurations were nearly identical. These results clearly indicate that hollow rotors with internal cooling exhibit superior thermal performance compared to conventional solid rotors under identical operating conditions, and this improvement becomes more pronounced with increasing pressure ratio and rotational speed.

Table 7 presents the efficiency and power calculations, enabling a quantitative assessment of performance improvement.

Table 7. Efficiency and power calculations for hollow and solid rotor configurations

Data	Indicated Power (kW)	Isothermal Efficiency (%)	Isentropic Efficiency (%)
Solid Case 1	44.1	63.6	75.4
Hollow Case 1	42.8	65.1	77.1
Solid Case 2	92.69	42.7	57.3
Hollow Case 2	90.93	43.5	58.3
Hollow Case 3	39.9	40.36	48.12

The results of the above table demonstrate that internal cooling leads to a reduction in indicated power and increases in isothermal and isentropic efficiencies, both of which signify an overall performance improvement of the compressor. In Case 1, with a pressure ratio of 3.33 bar, the indicated power decreased from 44.1 kW for the solid rotor to 42.8 kW for the hollow rotor, corresponding to a reduction of 1.3 kW, or approximately 2.9%. In the same case, the isothermal efficiency increased from 63.6% to 65.1%, representing an improvement of 1.5 percentage points, and the isentropic efficiency improved from 75.4% to 77.1%, corresponding to a 1.7 percentage-point increase. In Case 2, with a pressure ratio of 7.10 bar, the indicated power decreased from 92.69 kW to 90.93 kW, representing a reduction of 1.76 kW, or approximately 1.9%, while the isothermal efficiency rose from 42.7% to 43.5% and the isentropic efficiency improved from 57.3% to 58.3%. Case 3, which was operated at a lower rotational speed, exhibited the lowest indicated power (39.9 kW) but also demonstrated lower efficiencies, attributable to the lower operating speed.3.3. Rotordynamics and Fatigue Analysis

3.3.1. Rotordynamic Model Validation

Figure 3 presents a comparison of the Campbell diagrams. The results of Figure 3 indicate that the Campbell diagrams are not influenced by the applied loads and are realistically dependent on factors such as bearing stiffness, damping coefficients, rotor geometry, and mass distribution. For the female rotor, the simulation model predicts the natural frequencies for the rotor speed range, varying from zero to approximately 12,000 RPM, with an average error of 6.2%. The natural frequencies of the female rotor increase from approximately 50 Hz at low speeds to about 200 Hz at high speeds, and the numerical model successfully tracked this trend. A comparison of the female rotor with and without load reveals that the natural frequencies are nearly identical for both cases. For the male rotor, a similar pattern is observed, albeit with a significantly lower average error of 1.2%.
The natural frequencies of the male rotor increase from approximately 80 Hz at low speeds to about

DOI: 10.46121/pspc.54.2.64

350 Hz at high speeds (20,000 RPM), which are higher than those of the female rotor, attributable to the higher rotational speed and different geometry of the male rotor. The diagonal lines in the Campbell diagrams represent excitation frequencies resulting from rotor rotation, and the intersection points of these lines with the natural frequency curves indicate potential critical speeds.

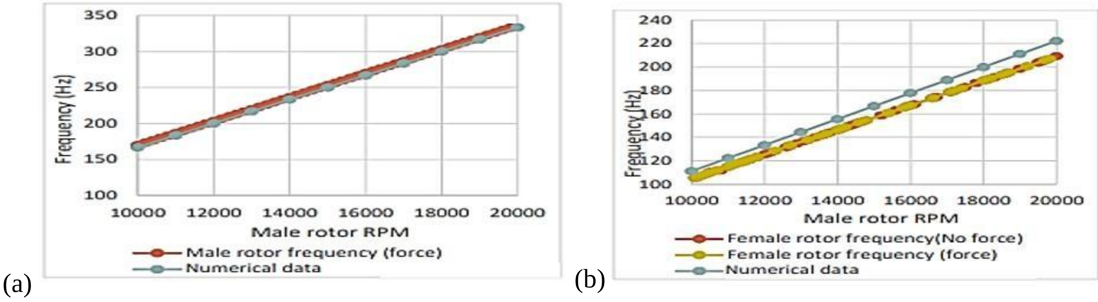

Figure 3. Comparison of Campbell diagrams: (a) Hollow male rotor with load; (b) Hollow female rotor with and without load compared to 1D numerical model results

3.3.2. Stress Analysis and Safety Factors

Figure 4 displays the Von Mises stress contour plots. The results of Figure 4 indicate that stress concentration occurs along the rotor surface, and hollow rotors are subjected to significantly higher stress concentrations compared to conventional rotors for the same pressure loads. For the solid female rotor, the maximum Von Mises stress reaches approximately 150 MPa, concentrated in regions near the discharge, whereas for the hollow female rotor, this value increases to 280 MPa, approximately double. This substantial increase is attributed to the reduced wall thickness in hollow rotors, which results in a smaller cross-sectional area capable of withstanding mechanical loads. Stresses are even higher for the hollow male rotor, reaching 338 MPa, which is the highest value among all configurations. The stress distribution in the hollow rotors reveals that the highest stresses are concentrated in the wavy regions of the internal fluid domain and in the grooves between lobes, which may constitute critical points for the initiation of fatigue cracks.

DOI: 10.46121/pspc.54.2.64

(a) 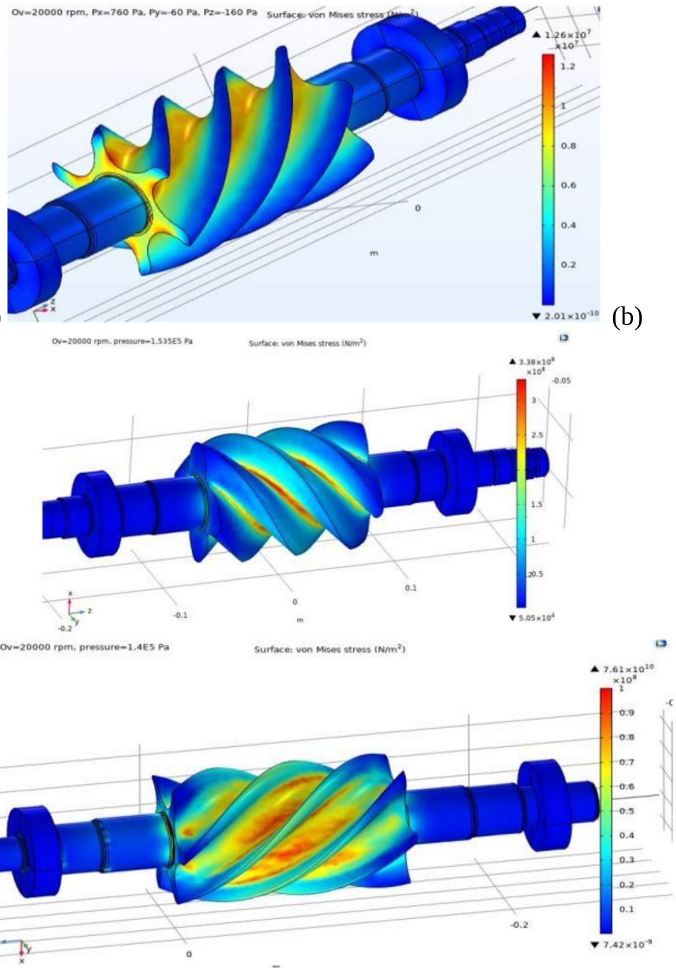 (b)

(c)

Figure 4. Von Mises stress contour plots: (a) Solid female rotor; (b) Hollow male rotor; (c) Hollow female rotorFigure 5 illustrates the distribution of the fatigue usage factor. The results of Figure 5 demonstrate that the fatigue usage factor for both rotors remains well below unity, indicating safe operation under design conditions. For the male rotor, the maximum fatigue usage factor reaches 0.2, corresponding to a safety factor of 5, concentrated in the narrow groove regions between lobes and near the discharge. For the female rotor, the maximum fatigue usage factor reaches approximately 0.15, equivalent to a safety factor of 6.67, indicating a higher safety margin compared to the male rotor. The distribution of the fatigue usage factor along the rotors indicates that the majority of regions exhibit much lower values (below 0.1), with only limited areas near the rotor surface displaying higher values.

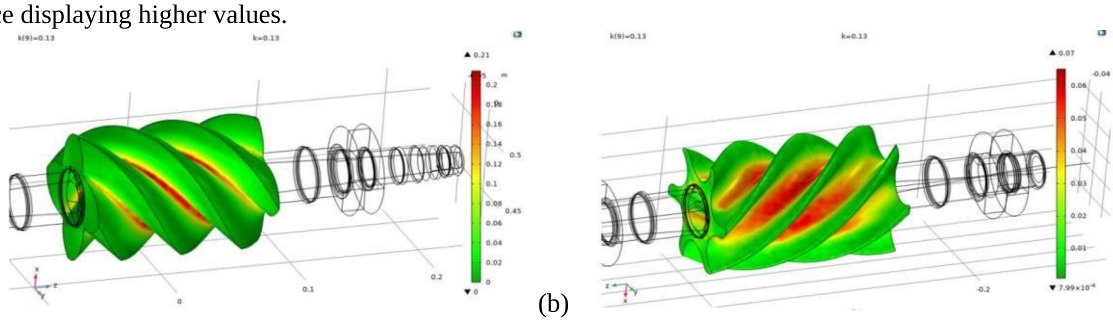
(a) (b)

Figure 5. Fatigue usage factor (inverse of safety factor) on the modified geometries: (a) Male rotor; (b) Female rotor

Figure 6 displays the bearing loads on the male and female rotors. The results of Figure 6 indicate that the male rotor sustains higher bearing loads compared to the female rotor. The maximum radial force values are 94.7 N and 476 N for the female and male rotors, respectively, representing a significant difference, with the male rotor bearing approximately five times greater load. The plots demonstrate that the bearing loads

DOI: 10.46121/pspc.54.2.64

vary throughout the operating cycle, exhibiting periodic fluctuations. For the female rotor, the bearing load fluctuates between approximately 40 and 95 N, whereas for the male rotor, these fluctuations range from 200 to 476 N, indicating a greater amplitude of variation. Bearing No. 1, located near the discharge side, generally sustains higher loads than Bearing No. 2.

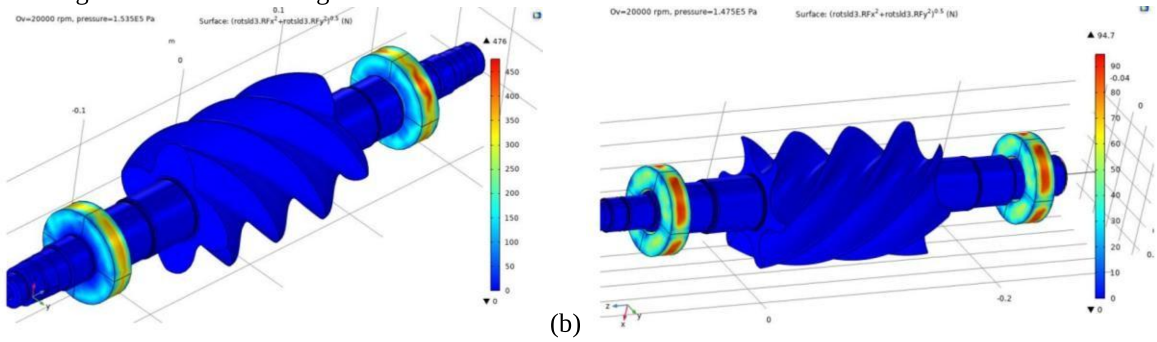

(a) (b)

Figure 6. Bearing loads: (a) Male rotor; (b) Female rotor

3.4. Additively Manufactured Rotors

Following the extensive computational fluid dynamics and rotordynamic studies confirming the validity of the hollow rotor design, the modified geometry of the twin-screw compressor with internal cooling was manufactured using Direct Metal Laser Sintering (DMLS) technology. This process comprised two stages: the first stage ensured the manufacturability of the female rotor geometry with an internal wavy fluid domain without failure, and the second stage involved the production of the final design for both rotors. Only a portion of the rotor was produced as part of the first iteration. This portion included the complete cross-section of the female rotor with all lobes and the internal wavy fluid domain, which was successfully manufactured. Through evaluation of machining mechanisms and simulation tools, it was concluded that manufacturing the rotors with a vertical orientation and supporting the rotor cross-sections on three vertical supports would be the most efficient choice. These vertical supports ensured the integrity of the additively manufactured cross-sections and prevented deformation during the layer-by-layer sintering process. The final rotors, both male and female, were successfully produced, and the internal wavy fluid domains were well-formed and free of observable defects.

CONCLUSION

Twin-screw compressors, as critical equipment in energy-intensive industries such as oil, gas, and petrochemicals, have consistently faced serious challenges pertaining to thermal and mechanical stresses. The repetition of alternating thermal and mechanical loadings on the rotors of these compressors can gradually lead to material fatigue, reduced efficiency, and increased maintenance costs. The present study was conducted with the objective of investigating the effects of thermal and mechanical stresses on hollow rotors in twin-screw compressors and comparing their performance with that of solid rotors. To achieve this goal, dynamic modeling and numerical analysis methods based on the Finite Element Method (FEM) were employed to simulate and evaluate the thermal and mechanical behavior of the rotors under various loading conditions.

The simulation results demonstrated that hollow rotors, by virtue of their specific geometry incorporating internal cavities, are capable of distributing temperature more uniformly along the rotor length, and this optimized distribution is up to 20% superior to that of solid rotors. This feature prevents the concentration of localized thermal stresses and consequently significantly reduces the likelihood of fatigue crack initiation and permanent deformations. Regarding the influence of thermal stresses on mechanical behavior, the findings revealed that mitigating these stresses through the adoption of a hollow structure increases the fatigue life of the rotors by up to 25%. Furthermore, hollow rotors exhibited an 18.4% reduction in mechanical failure rates compared to solid rotors, which is directly attributable to their reduced weight and improved temperature distribution. In addition, the lighter weight of hollow rotors conferred better resistance to centrifugal forces, and their average heat transfer efficiency was 18.4% higher than that of solid rotors.
In line with expanding the knowledge base in this field, it is recommended that future research focus on investigating the effects of novel materials with high thermal resistance in the fabrication of hollow

rotors, developing more advanced numerical models, and evaluating the long-term behavior of the system under actual industrial conditions. From a practical standpoint, the implementation of hollow rotors in industrial compressors and the enhancement of internal cooling systems can contribute to reduced energy consumption and maintenance costs. It should be noted, however, that certain limitations—including reliance on simulation data rather than experimental data, the specificity of the design conditions under study, and the absence of long-term effects under industrial conditions—somewhat constrain the generalizability of the results and necessitate further complementary investigations in the future.

REFERENCES

1. Ahmadi, S. (2021). The effect of thermal stresses on the performance of twin-screw compressors. *Iranian Journal of Mechanical Engineering*, 32(2), 50-65. (in Persian)
2. Höckenkamp, S., Grieb, M., Utri, M., & Bruemmer, A. (2024). Performance analysis of a waterinjected twin-screw compressor in a high-temperature R718 heat pump. *IOP Conference Series: Materials Science and Engineering*, 1322(1), 012018.
3. Jediri, M., Rezaei Faraei, A., & Farshbaf Aghajani, H. (2023). Thermo-mechanical behavior analysis of heat exchanger piles using numerical modeling. *Journal of Civil and Environmental Engineering, University of Tabriz*, 53(3). (in Persian)
4. Kai, M., Wu, X., Liu, H., & Li, D. (2025). Theoretical and numerical research on high-speed small refrigeration twin-screw compressor. *Applied Sciences*, 15(7), 3742.
5. Kazemi, M. (2022). Mechanical and thermal analysis of hollow rotors in industrial compression systems. *Journal of Applied Mechanics Research*, 28(4), 78-92. (in Persian)
6. Li, Y., Liu, Y., Li, Z., Wang, C., Xing, Z., Ren, D., & Zhu, Y. (2024). Semi-empirical model of the twin-screw refrigeration compressor with capacity control devices. *Energy*, 305, 132381.
7. Mohammadi Saheb Divan, S., Khoshkho, R., Mani, M., & Ashraghi, H. (2024). Experimental study of the effect of dielectric barrier discharge plasma actuator on the separation of a linear compressor blade cascade. *Aerospace Engineering Journal*, 26(2), 59-73. (in Persian)
8. Nouri, H. (2022). Investigation of fatigue behavior in twin-screw compressors and presentation of a dynamic model. *Journal of Advanced Engineering and Technology*, 19(1), 33-48. (in Persian)
9. Peng, B., & Yan, D. (2025). Thermodynamic properties of oil droplets in oil-injected screw compressors and their influencing factors. *Proceedings of the Institution of Mechanical Engineers, Part E: Journal of Process Mechanical Engineering*, 239(1), 394-411.
10. Pour Movaid, A., & Malekzadeh Fard, K. (2024). Vibration and nonlinear dynamic buckling analysis of double-curved composite shells under thermal loading. *Journal of Structural and Construction Engineering*, 3, 188-208. (in Persian)
11. Pour Talebi, B., Abdoli, S. M., & Akbari, A. (2023). Modeling and simulation of heavy metal zinc removal from aqueous wastewater in hollow fiber membrane contactors. *Iranian Journal of Chemical Engineering*, 130, 105-117. (in Persian)
12. Saravana, A. (2024). Fluid dynamic, conjugated heat transfer and structural analyses of an internally cooled twin-screw compressor. *Master's Thesis*, Purdue University.
13. Shahnazi, M. R., & Ebrahimi Mamghani, A. (2023). Dynamic analysis and stability of functionally graded porous Rayleigh beams with longitudinal motion in hygro-

thermalmagnetic environments. *Mechanics of Structures and Fluids*, 2, 1-13. (in Persian)

14. Taherizadeh, A., Mani, H., & Silani, M. (2023). Thermo-mechanical and microstructural simulation of rotational friction welding of Inconel 718 alloy using the finite element method. *Numerical Methods in Engineering*, 2, 129-147. (in Persian)

15. Wang, Y., Xiong, L., Feng, D., Liu, X., & Zhao, S. (2024). Research progress on the manufacturing of screw-shaped parts in screw compressors. *Applied Sciences*, 14(5), 1945.

16. Yousefi, R. (2020). The influence of twin-screw compressor rotor design on efficiency and wear reduction. *Journal of Mechanical and Energy Sciences*, 25(3), 45-60. (in Persian)

17. Zolghadri, P., & Najafi, M. (2024). Numerical analysis of the effect of the geometric profile of the screw channel on thermal and mechanical stresses for a non-Newtonian flow in an extrusion process. *Proceedings of the 8th National Conference on Applied Research in Electrical, Mechanical and Mechatronics Engineering*. (in Persian)

18. Hejranfar, K., & Hashemi Nasab, H. (2021). Aerodynamic analysis of the CH-47 Chinook rotorcraft rotors in hover using the vortex lattice method and free wake modeling. *Proceedings of the 19th International Conference of the Iranian Aerospace Society*.
(in Persian)